ACS APPLIED MATERIALS & INTERFACES

Research Article

www.acsami.org

General Method for the Synthesis of Hollow Mesoporous Carbon Spheres with Tunable Textural Properties

Stefano Mezzavilla,[†] Claudio Baldizzone,[‡] Karl J. J. Mayrhofer,[‡] and Ferdi Schüth*[,†]

[†]Department of Heterogeneous Catalysis, Max-Planck-Institut für Kohlenforschung, Kaiser-Wilhelm-Platz 1, 45470 Mülheim an der Ruhr, Germany

[‡]Department of Interface Chemistry and Surface Engineering, Max-Planck-Institut für Eisenforschung GmbH, Max-Planck-Strasse 1, 40237 Düsseldorf, Germany

Supporting Information

ABSTRACT: A versatile synthetic procedure to prepare hollow mesoporous carbon spheres (HMCS) is presented here. This approach is based on the deposition of a homogeneous hybrid polymer/silica composite shell on the outer surface of silica spheres through the surfactant-assisted simultaneous polycondensation of silica and polymer precursors in a colloidal suspension. Such composite materials can be further processed to give hollow mesoporous carbon spheres. The flexibility of this method allows for independent control of the morphological (i.e., core diameter and shell thickness) and textural features of the carbon spheres. In particular, it is demonstrated that the size of the pores within the mesoporous shell can be precisely tailored over an extended range (2−20 nm) by simply adjusting the reaction conditions. In a similar fashion, also the specific carbon surface area as well as the total shell porosity can be tuned. Most importantly, the textural features can be adjusted without affecting the dimension or the morphology of the spheres. The possibility to directly modify the shell textural properties by varying the synthetic parameters in a scalable process represents a distinct asset over the multistep hard-templating (nanocasting) routes. As an exemplary application, Pt nanoparticles were encapsulated in the mesoporous shell of HMCS. The resulting Pt@HMCS catalyst showed an enhanced stability during the oxygen reduction reaction, one of the most important reactions in electrocatalysis. This new synthetic procedure could allow the expansion, perhaps even beyond the lab-scale, of advanced carbon nanostructured supports for applications in catalysis.

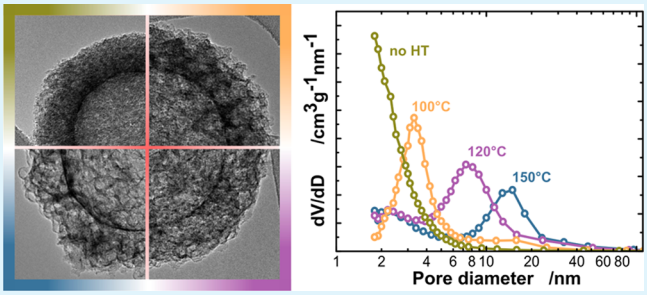

KEYWORDS: *mesoporous materials, hollow mesoporous carbon spheres, pore size, tunable textural properties, oxygen reduction reaction*

INTRODUCTION

Over the past decades, hollow mesoporous spheres have received considerable attention for their interesting properties in many fields of heterogeneous catalysis[1] and as platforms for drug delivery.[2] Among this large family of nanostructured materials, hollow mesoporous carbon spheres (HMCS) possess a broad spectrum of attractive characteristics, especially for energy-conversion/storage applications where electronic conductivity is often required. Indeed, the two major components of such structures, i.e., the hollow central cavity and the mesoporous shell, can offer a versatile set of functional options. In particular, it is possible to envision the hollow core as a nanoreactor capable to host (metal) nanoparticles[3−5] or as a reservoir for reactants.[6] Also, when the cavity is not hosting any active species, it is generally believed that it may improve the diffusion of reactants and products through the catalyst bed or electrode.[7,8] The second component, the mesoporous shell, can play an important role by acting as a physical separation between the nanoreactors and thus improving the catalyst stability,[9−11] but it can also be used to encapsulate metallic nanoparticles.[12,13] Hence, the functional multiplicity of HMCS makes such structures a very versatile platform for many applications.

Although soft-templating methods can be effectively adopted to prepare hollow carbon spheres, the resulting shells are, in most cases, microporous, and the possibilities to tune their textural properties are very limited.[14] Up to now, the most robust strategy to prepare HMCS remains the hard-templating (nanocasting) process using solid core mesoporous shell (SCMS) silica spheres as exotemplate.[15,16] However, also with this approach the range of achievable pore sizes is rather restricted. In fact, the porosity is indirectly determined by the textural properties of the preformed exotemplate, which can typically be adjusted only within a limited window (2−5 nm).[14,17−19] In addition, the nanocasting process is not easily scalable, as several synthetic steps are necessary even to prepare

Received: March 24, 2015
Accepted: May 19, 2015
Published: May 19, 2015

DOI: 10.1021/acsami.5b02580
ACS Appl. Mater. Interfaces 2015, 7, 12914−12922

the template for the impregnation. In this respect, the synthesis of HMCS, and mesoporous carbons in general, via hard-templating methods would be greatly simplified if the exotemplate skeleton and the carbon precursors were simultaneously deposited to form a hybrid nanocomposite. This is particularly important, since difficulties in the synthesis of multigram or even multitengram amounts of the hollow spheres are one of the most severe obstacles for further exploitation of concepts for fuel cell catalysts based on hollow graphitic carbon spheres.[13,20]

The numerous mechanistic parallels between alkoxysilane hydrolysis−condensation reactions and resorcinol−formaldehyde (RF) base-catalyzed polymerization led many researchers to the development of synthetic procedures to concurrently polymerize silica precursors and RF resins. Following this strategy, bulk polymer/silica hybrid ceramics,[21,22] nanocomposites,[23,24] and aerogels[25] were synthesized. In a similar fashion, the Zhao group has introduced a family of 2D[6] and 3D[26] ordered mesoporous polymer/silica and carbon/silica nanostructures and films[27] via the surfactant-assisted simultaneous polycondensation of low molecular weight phenolic resins (resols) and tetraethylorthosilicate (TEOS). Recently, on the basis of the new Stöber-like process introduced by Liu et al.[28] to synthesize RF colloidal spheres, Zhang et al.,[29] Qiao et al.[30] and Wang et al.[31] developed methods to prepare mesoporous carbon structures (nonspherical, core−shell, and yolk−shell) via the homogeneous simultaneous polycondensation of TEOS and RF.

Herein, we introduce a generalized and versatile synthetic procedure to prepare hollow mesoporous carbon spheres (HMCS) through the deposition of a nanocomposite polymer/silica shell on the outer surface of silica spheres, via the simultaneous polycondensation of TEOS and RF. These core−shell hybrid spheres can be transformed into HMCS via carbonization and subsequent removal of the silica template. The textural properties of the carbon shell, i.e., total pore volume and pore size, can be precisely tailored over an extended range by simply adjusting the conditions employed during the synthesis.

RESULTS AND DISCUSSION

Synthesis Description. The HMCS synthesis can be conceptually divided into four steps. (1) Initially, colloidal silica spheres (∼200 nm) are prepared via a Stöber method. The spheres diameter can easily be tailored, as known for the Stöber process.[32] (2) At this stage, the reaction mixture composition is adjusted (without separation of the colloidal particles) to initiate the deposition of a polymer/silica nanocomposite shell. The key idea behind the formation of the hybrid shell is the heterogeneous nucleation of a biphasic polymer/silica nanocomposite layer through the surfactant-assisted simultaneous polycondensation of RF and TEOS. At the end of this phase, the colloidal spheres (Figure 1a) consist of a silica core and a silica/RF shell (70−80 nm). Afterward, (3) the reaction mixture is hydrothermally treated. Only after this step, the solid phase is separated, and (4) it is further carbonized (Figure 1b). Hollow mesoporous carbon spheres are finally obtained through the removal of the silica scaffold (Figure 1c−f). During the formation of the nanocomposite shell, each element of the reaction mixture, resorcinol (R), formaldehyde (F), TEOS (T), and CTAC, plays an active role: if any of the reactants is absent, the synthesis is not successful. The shell volume, and inherently the thickness of the final mesoporous carbon shell, can easily be tuned by adjusting the initial total amount of reactants, without altering the final carbon textural properties. Figure 1f exemplarily shows the HMCS obtained after doubling the concentration of the reactants and CTAC (75.5 mM for R + T and 118 mM for CTAC). The shell thickness increased from ∼60 nm (Figure 1e) to ∼110 nm.

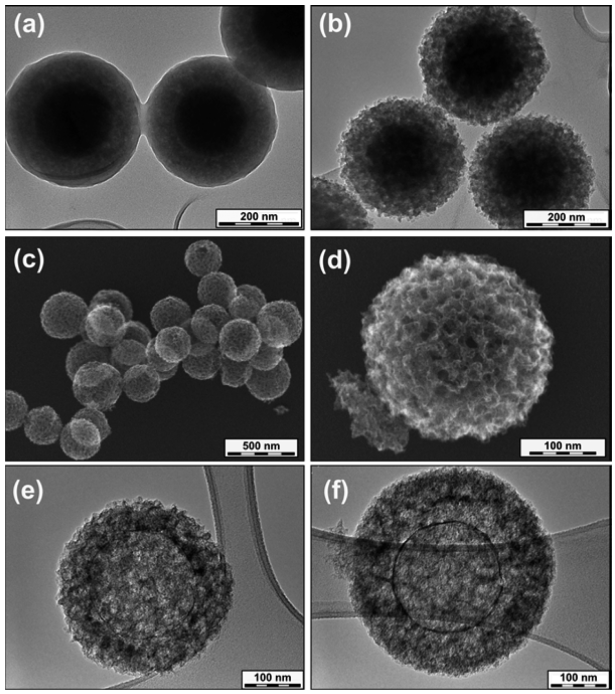

Figure 1. Transmission electron microscopy (TEM) and scanning electron microscopy (SEM) images of the spheres at different stages during the synthesis: (a) silica@polymer/silica after the hydrothermal treatment; (b) silica@carbon/silica after the carbonization step; (c−f) SEM and TEM images of HMCS after the silica leaching. (e, f) Examples of HMCS prepared using the standard conditions (e) and with a double concentration of reactants and CTAC (f). For both of them the silica core had a diameter of ∼200 nm.

The silica shell framework formed during the simultaneous condensation has the crucial function to preserve and control (as discussed later) the mesoporosity within the carbon shell, thus acting as scaffold for the polymer and carbon. In particular, it plays a fundamental role during the carbonization step when it strongly decreases the shell shrinkage. The same structure was found to be decisive in the formation of ordered mesoporous carbon/silica composites.[33]

Influence of the Hydrothermal Treatment (HT) and Formation Mechanism. In many cases, especially for silica-based materials, hydrothermal treatments have often been used to tailor the textural properties (i.e., porosity, pore size, morphology) of silica-gels[34] and ordered micelle-templated mesoporous materials (MCM-41 or SBA-15).[35] In a similar fashion, comparable treatments have extensively been applied to synthesize and to control the properties of phenol−formaldeyde sol−gel nanostructures.[36,37] Originally, Liu et al. applied a HT (100 °C for 24 h) as the final step of the synthetic procedure to prepare RF spheres through a Stöber-like process.[28] However, it is still unclear, according to the partially conflicting reports in related studies,[30,38−41] what impact has the HT on the polymer/carbon chemical and textural properties. We thus decided to study the effect of the HT on our polymer/silica composite nanostructure in more detail,

DOI: 10.1021/acsami.5b02580
ACS Appl. Mater. Interfaces 2015, 7, 12914−12922

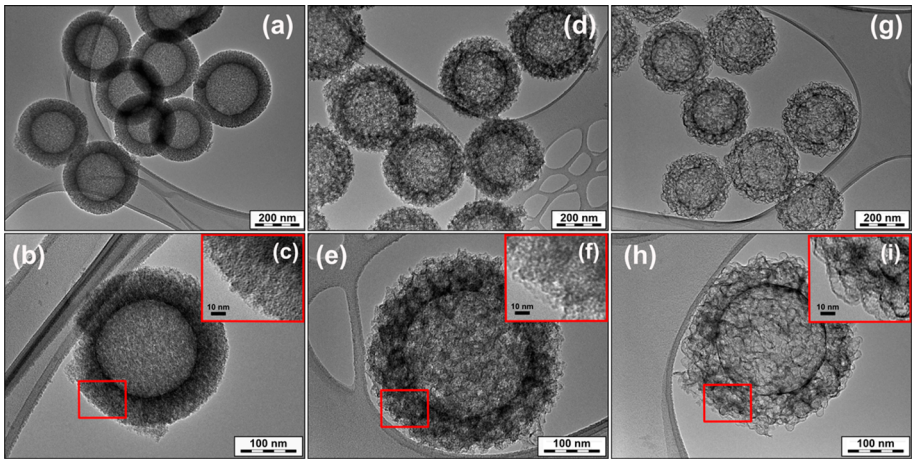

Figure 2. Transmission electron microscopy (TEM) images of HMCS obtained by treating polymer/silica spheres at different HT temperatures. The images were taken after carbonization and the leaching of the silica framework: (a–c) HMCS-noHT, (d–f) HMCS-100, (g–i) HMCS-150. For space reasons, the images relative to HMCS-120 are not shown.

with special attention to the HT temperature. The core–shell spheres obtained after the deposition of the nanocomposite shell were therefore treated at three different HT temperatures (100, 120, and 150 °C, all of them in the mother liquor), and we studied the properties of the resulting silica and carbon spheres. In addition, a fourth sample was not hydrothermally treated. All samples were prepared from the same starting batch, so that the differences among them can be attributed only to the different HT temperatures.

In our case the HT temperature has a decisive effect on the textural properties of both the carbon (Figure 2) and silica mesoporous structures. Although both the spherical morphology and size of the HMCS are unaffected by the different treatments, the materials present very different textural features. As visible in the magnified images (Figure 2c,f,i), HMCS-100 and HMCS-150 show a much more open structure with large (especially for HMCS-150) interconnected pores.

The N_2 physisorption analysis (Figure 3a,b and Table 1) shows that all four materials present type IV isotherms with an important microporous contribution ($p/p_0 < 0.1$) and an H2-type hysteresis loop (less pronounced for HMCS-noHT), which points to an ink-bottle-type pore morphology. The delayed evaporation responsible for the asymmetric hysteresis can be ascribed both to cavitation (tensile-strength effect) and pore-blocking effects. A more comprehensive discussion of this point is reported in the Supporting Information (Figure S2). To avoid artifacts, all the reported pore size distribution (PSD) curves are therefore calculated applying the BJH method to the isotherm adsorption branch. Although this method typically underestimates the average pore size,[42] it is used for comparison between the materials, since the differences are most important and the error by the tensile strength effect, which would be introduced by using desorption data, seemed to be more severe. For HMCS-noHT (Figure 3b), the average pore size is below 2 nm, and it progressively increases to 3.8 nm for HMCS-100, 7.3 nm for HMCS-120, and 13.9 nm for HMCS-150. The number of pores, expressed by the intensity of the PSD curves, progressively decreases when higher HT temperatures are applied, as if an internal reconstruction was taking place and fewer large pores grew at the expenses of a porous network made by small (micro)pores. As a further indication of such rearrangement, the BET specific surface areas (see Table 1) constantly decrease (from 2385 m^2/g for HMCS-noHT to 916 m^2/g for HMCS-150) upon increasing HT temperature. The textural evolution evidenced by the PSDs is confirmed by the progressive shift of the condensation hysteresis loop in the adsorption isotherms upon increasing HT temperature. The absence of a plateau at high relative pressures ($p/p_0 \sim 1$) is due to the condensation occurring in

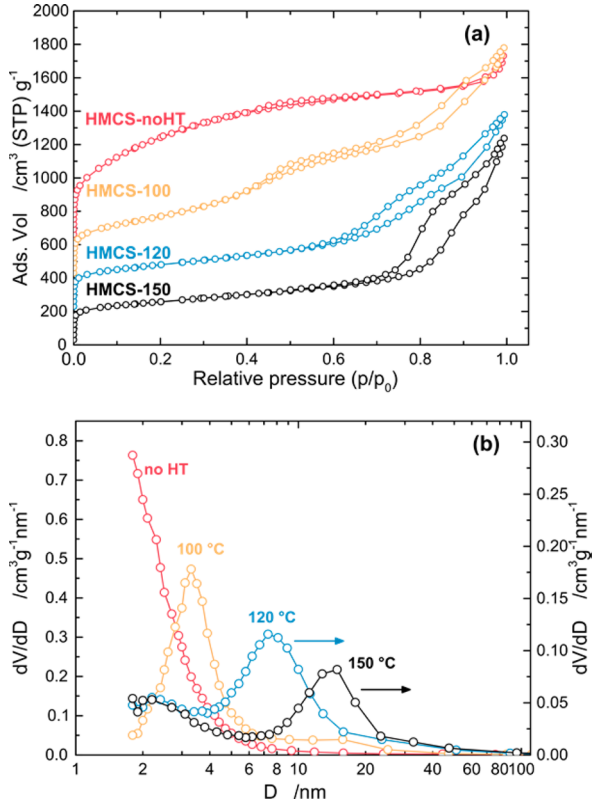

Figure 3. Influence of the hydrothermal treatment (HT) on the HMCS textural properties. (a) N_2 physisorption isotherms for HMCS obtained applying different HT temperatures. The isotherms for HMCS-noHT, HMCS-100, and HMCS-120 are vertically shifted by 600, 400, and 200 cm^3/g, respectively. (b) Corresponding pore size distributions (PSDs) calculated applying the BJH method to the adsorption branch. The curves for HMCS-120 and HMCS-150 refer to the right *y*-axis.

DOI: 10.1021/acsami.5b02580
ACS Appl. Mater. Interfaces 2015, 7, 12914–12922

Table 1. Textural Properties and Average Diameter of Hollow Mesoporous Carbon Spheres (HMCS) Obtained Applying Different HT Temperatures and T/R Ratios

sample	S_{BET}[a] ($m^2\ g^{-1}$)	TPV[b] ($cm^3\ g^{-1}$)	D_p[c] (nm)	avg. diameter[d] (nm)
HT Temperature				
HMCS-noHT	2385	1.75	<2	284 ± 22
HMCS-100 (and HMCS T/R-2)	1319	2.13	3.8	304 ± 24
HMCS-120	990	1.82	7.3	290 ± 24
HMCS-150	916	1.91	13.9	303 ± 21
T/R Ratio				
HMCS-T/R-1	823	0.83	3−4	
HMCS-T/R-1.5	1080	1.49	3−4 and 15	
HMCS-T/-3.5	1404	2.26	3−4 and 15	

[a]BET specific surface area. [b]Total pore volume determined from the N_2 uptake at the relative pressure (p/p_0) of 0.98. [c]Pore diameter (maximum of the pore size distribution curve obtained from the isotherm adsorption branch). [d]Average outer diameter of the sphere calculated from TEM micrographs of more than 200 spheres.

the interparticle voids and/or to the roughness present on the outer surface of the spheres. These phenomena are more pronounced for the samples HMCS-100, HMCS-120, and HMCS-150 compared to HMCS-noHT (Figure 1c,d).

The mechanism behind the textural reconstruction occurring in the polymer/silica shell becomes clear if one observes the evolution of the silica counterpart at different HT temperatures. In this case, a portion of the same samples used to obtain HMCS was isolated before the carbonization, and a simple calcination in air (600 °C, 2 °C/min) was carried out to remove the polymeric phase. All the obtained samples consist of solid core mesoporous shell (SCMS) spheres (Figure 4). Although (as for HMCS) the overall spherical morphology is retained during the HT, a substantial textural evolution is evident within the porous shell.

The progressive coarsening of the silica primary units leads to a reconstruction of the porous network upon increasing the HT temperature. The average size of the primary units increases from about 1−2 nm in the case of SCMS-noHT, to 4−6 nm for SCMS-100, 8−10 nm for SCMS-120, and 15−20 nm for SCMS-150. The sizes of the silica primary units match the average pore sizes of the corresponding HMCS, indicating that the silica framework is not only responsible for preservation of the mesoporosity during carbonization, but it directly controls the average pore size of the carbon replicas. The qualitative trend revealed by the TEM images is confirmed by the quantitative N_2 physisorption analysis (Supporting Information Table S1 and Figure S1). The TEM analysis reveals also the formation of a yolk−shell structure as consequence of the HT (SCMS-100 and SCMS-150 in Figure 4). In order to obtain information on the origin of this effect, more than 200 different spheres were analyzed. Since the core average size (200 ± 20 nm) remains unchanged during the HT, it can be excluded that the space between the core and the shell is formed as the consequence of the base-catalyzed (NH_3) dissolution of the outer portion of the silica core, as reported in other cases.[43,44] In contrast, it seems that the expansion of the shell during the HT is responsible for the formation of the yolk−shell structure.

On the basis of these phenomenological observations, we propose the following mechanism (Scheme 1) for the formation of the shell. (1) As soon as it is added to the reaction mixture, TEOS is quickly hydrolyzed to form negatively charged silicates, and formaldehyde immediately reacts with resorcinol to form (di)methylol resorcinols and quinone methide species.[45] Both resorcinol and silicate oligomers can electrostatically interact with the positively charged trimethylammonium cation (CTAC). Considering that the CTAC concentration (15 mM) is below the critical micelle concentration (CMC) for comparable ethanol−water mixtures,[46,47] it is unlikely that surfactant micelles are present before this stage. (2) The interconnected CTAC and silicate−resorcinol oligomers will diffuse to the surface of the silica spheres due to the electrostatic interaction with NH_4^+ cations that cover the outer surface of the silica colloids, as previous studies have suggested.[28,38] Through such a cooperative process, the oligomers will further condense and cross-link to develop a composite shell. Zhang et al.[29] and Qiao et al.[30] have previously suggested that the ethanol/water ratio controls the relative rate between silica and RF polycondensations. In the present case, we found that an ethanol/water ratio equal to 0.5 (v/v) is ideal to achieve an optimal balance between the rates of the two reactions. Consequently a homogeneous biphasic

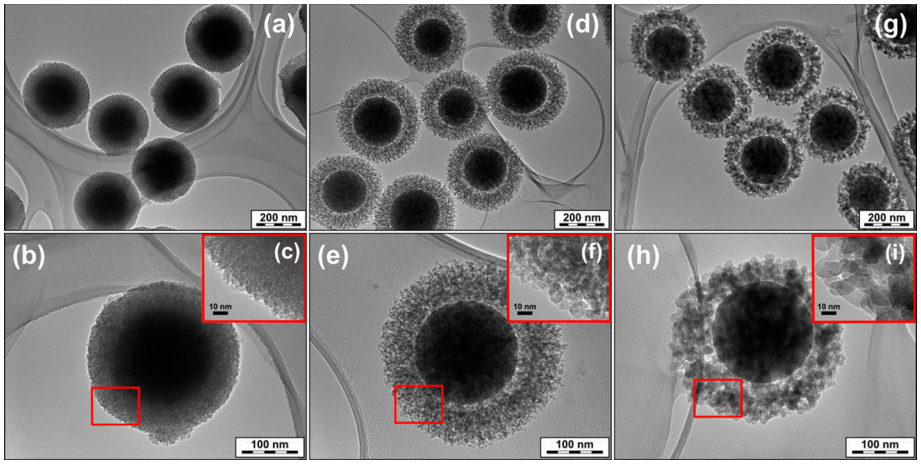

Figure 4. Transmission electron microscopy (TEM) images of SCMS silica spheres obtained by calcination in air of the polymer/silica spheres previously treated at different HT temperatures: (a−c) SCMS-noHT, (d−f) SCMS-100, (g−i) SCMS-150. The sample SCMS-120 is not shown.

DOI: 10.1021/acsami.5b02580
ACS Appl. Mater. Interfaces 2015, 7, 12914−12922

Scheme 1. Shell Formation Scheme[a]

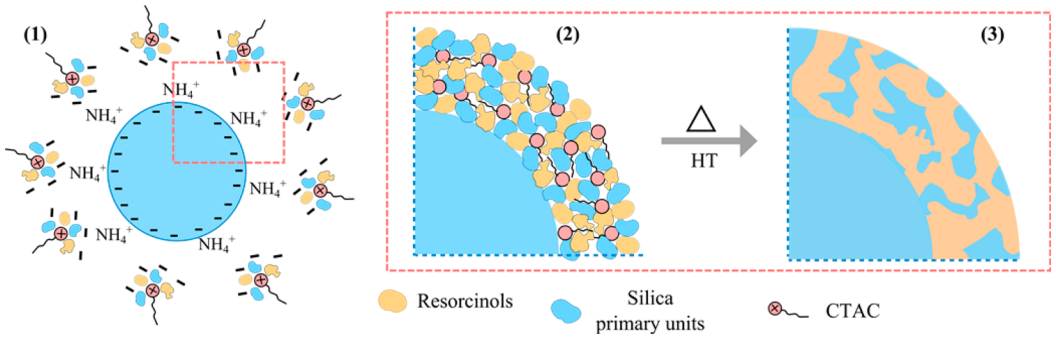

[a](1) Electrostatic interactions between resorcinol/silica primary units/CTAC, and between such clusters and the surface of the nonporous silica cores. (2) Simultaneous polycondensation (mediated by CTAC) of polymeric and silica primary units. (3) Reconstruction of the hybrid composite shell during the hydrothermal treatment (HT).

silica/polymer composite shell is formed. (3) During the HT, a progressive coarsening of the silica framework takes place. It is likely that such evolution is induced by a local dissolution–precipitation mechanism driven by an Ostwald-ripening-type process where the silica primary units merge and grow due to the presence of a local solubility gradient. This process typically occurs for porous sol–gel silica under similar conditions,[48] and it was previously reported for ordered polymer/silica nanostructures.[33] Most likely, the yolk–shell structure visible in the silica SCMS spheres (Figure 4) is formed in this step. There are different possible reasons for the formation of such structure, but presently we do not have sufficient experimental evidence to support one or the other. On the basis of thermogravimetrical analysis (Supporting Information Figure S3), the HT seems to provide only a modest enhancement to the polymer thermal stability in air. Indeed, regardless of the HT temperature, all the samples present comparable weight losses and similar onset points in the degradation curves.

Influence of the TEOS/Resorcinol (T/R) Ratio. Given the number of reactants involved in the shell formation, it appears logical that the textural properties of the polymer/silica composite core–shell structures, and ultimately the HMCS properties, depend on a matrix of parameters (HT temperature, ethanol/water ratio, NH_3 concentration). Although each of them can potentially be tuned during the synthesis, we focused on the effect of the TEOS/resorcinol (T/R) ratio employed during the shell deposition. When the synthesis is governed by a homogeneous nucleation–growth mechanism as in the studies reported by Qiao et al.[30] and Wang et al.,[31] this parameter was found to be crucial in determining the final morphology and size of polymer/silica particles. In the case described here, the formation of the composite shell occurs via a heterogeneous nucleation–growth mechanism, since the silica colloids are already present in the reaction mixture. The T/R molar ratio used in the synthesis was correlated to the final HMCS textural properties. Specifically, the composite shell was deposited using four different T/R ratios: 3.5, 2, 1.5, and 1. All the samples, independently from the T/R ratio used, underwent the same HT (100 °C, 24 h); additionally, the amount of formaldehyde was maintained proportional to the amount of R used and the total reactant concentration (T + R) was kept constant.

The overall morphology of the hollow carbon spheres is retained irrespective of the ratio of the precursors (Supporting Information Figure S4). This is different from what has been reported for homogeneous nucleation–growth mechanisms where also the dimensions of the spherical structures change upon the variation of the T/R ratio.[31] The cumulative pore size distributions (Figure 5a and Table 1) reveal that the total pore volume (TPV) of the carbon shell progressively decreases upon decreasing the T/R ratio. At similar pore size and decreasing surface area, under the assumption of constant bulk carbon density, this means that the walls become thicker. In parallel, the TGA analysis (Figure 5b) confirms that the carbon/silica ratio (weight loss/residual weight) increases when the T/R

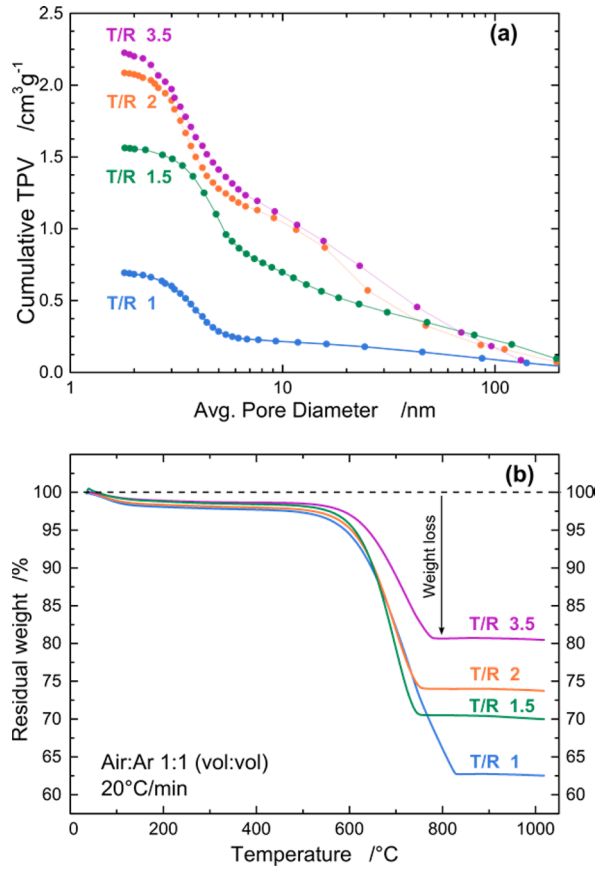

Figure 5. Influence of the T/R ratio on the HMCS textural properties. (a) Cumulative pore size distribution curves (adsorption branch) for HMCS synthesized using different T/R ratios. (b) TGA analysis of carbon/silica obtained with increasing T/R ratios.

DOI: 10.1021/acsami.5b02580
ACS Appl. Mater. Interfaces 2015, 7, 12914–12922

becomes smaller. It appears therefore clear that the T/R ratio controls the relative volume occupied by the silica and polymer phases within the shell composite, and it determines the final porosity of the carbon structure. By decreasing the T/R ratio, the volume occupied by the polymer phase is increased, and the resulting HMCS will possess thicker pore walls. Hence, the structure becomes less porous, and its specific surface area is reduced (see Table 1 and Supporting Information Figure S4). Following a similar logic, for large T/R ratio (>2) it is more likely that several silica primary units deposit next to each other during the shell formation, thus causing the growth of larger silica domains. Hence, in these cases, although the majority of the pores retain an average pore size of 3−4 nm, a small fraction of large pores (>10 nm) is present. In addition, the HMCS porous network becomes more fragile, leading to the shrinkage (T/R = 3.5) or complete collapse (T/R = 6, data not shown) of the shell.

Pt@HMCS as ORR Catalyst. Over the past years, our group has developed a family of active and stable oxygen reduction reaction (ORR) catalysts by encapsulating Pt and Pt alloys in the shell pores of hollow graphite spheres (HGS).[13,20] The unique HGS structure was found to be pivotal in assuring an optimal spatial distribution of the nanoparticles during the synthesis and in suppressing some of the catalyst degradation pathways, i.e., agglomeration and detachment.[13,49] However, especially to increase the amounts of material produced, a simpler and more scalable synthesis is urgently needed. The synthesis of the HMCS described in this work provides a very interesting alternative. In order to check the suitability of the new carbon structure for this application and, more generally, as an exemplary application of HMCS as support material, the ORR performance (stability/activity) of Pt@HGS and Pt@HMCS was compared. In both cases the metal nanoparticles were encapsulated in the mesoporous shell via an incipient wetness impregnation followed by a reduction-annealing treatment, as described in our previous work.[13]

The Pt nanoparticles are homogeneously dispersed within the mesoporous shell, and their average size is about 3−4 nm (Figure 6 and Supporting Information Figure S6). A more detailed comparison between the features of Pt@HGS and Pt@HMCS can be found in the Supporting Information. Following the method described in ref 20, PtNi nanoparticles also can be successfully encapsulated in HMCS. For Pt@HMCS, the measured specific activity (SA), mass activity (MA), and electrochemical surface area (ECSA) are 0.46 ± 0.12 mA/cm^2_{Pt}, 0.39 ± 0.1 A/mg_{Pt} and 85 ± 10 m^2/g_{Pt}, respectively. As expected, these values are comparable to the catalytic performance of Pt@HGS, since the two catalysts exhibit very similar Pt particle sizes. The SA values are in the expected activity range of conventional platinum catalysts with comparable size (see Supporting Information Table S2 and ref 50) indicating that once activated the catalyst active surface is fully accessible to the electrolyte and to reactants like oxygen. Hence, in the rotating disk electrode (RDE) setup, the presence of mass transport issues related to the mesoporous nature of the catalyst can be excluded. The stability of Pt@HMCS (Figure 6) was tested applying two accelerated-aging protocols (0.4−1.0 V_{RHE} and 0.4−1.4 V_{RHE}, both for 10 800 cycles with 1.0 V/s scan rate). The ECSA evolution was monitored via CO-stripping. The Pt@HMCS stability curve is comparable to the performance reported for Pt@HGS in both aging tests. Remarkably, especially in the 0.4−1.0 V_{RHE} degradation protocol, which mimics the potential excursions

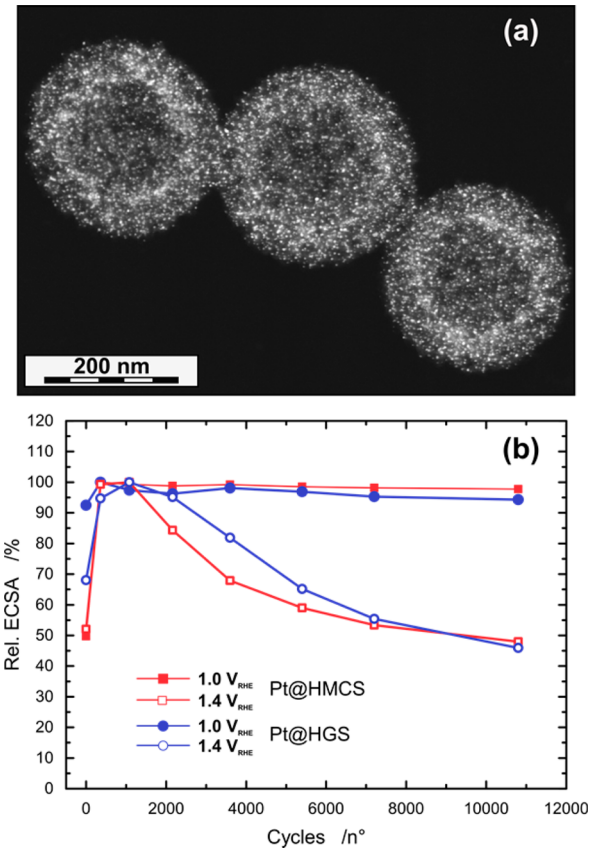

Figure 6. Electrochemical stability assessment for Pt@HMCS. (a) Dark-field STEM images of Pt@HMCS. (b) Relative ECSA monitored during two accelerated degradation tests (ADT) with different upper limit potentials, namely, V_{max} = 1.0 V_{RHE} and V_{max} = 1.4 V_{RHE}. For comparison, the ECSA curves for Pt@HGS (taken from ref 13) are also reported. At least three different measurements were recorded for every degradation test.

present in proton exchange membrane (PEM) fuel cells under normal operation conditions, the initial ECSA is fully retained over the entire period. Thus, equivalent to what was observed for Pt@HGS,[13,49] the pore-confinement effect prevents the nanoparticle from sintering, as instead occurs with Pt nanoparticles supported on conventional carbon supports.[51,52] We thus have developed a synthetic method which allows a much easier production of catalyst amounts sufficient for extended single cell tests.

CONCLUSIONS

A new synthetic procedure to prepare hollow mesoporous carbon spheres (HMCS) was successfully developed. The new synthetic approach bears multiple advantages. (i) It is a wet chemistry one-pot synthesis procedure to prepare core−shell silica/RF spheres that can replace the rather complex multistep nanocasting method previously employed.[15] (ii) The shell formation is based on a heterogeneous nucleation−growth process, and it takes advantage of the very good monodispersity assured by the initial "Stöber" process. Inherently, also the final HMCS exhibit an excellent quality. (iii) It is very versatile as both the size of the core and the volume of the shell can be adjusted in a broad range. (iv) The textural properties of the mesoporous shell (i.e., average pore size and TPV) can be easily tailored by changing the reaction composition/conditions. Such versatility, that was unattainable with conventional hard-

DOI: 10.1021/acsami.5b02580
ACS Appl. Mater. Interfaces 2015, 7, 12914−12922

templating methods, can be effectively exploited in the future for the synthesis of carbon supports with specific features. As an exemplary application of the new HMCS, platinum nanoparticles were encapsulated in the mesoporous shell. The resulting Pt@HMCS catalyst showed an enhanced stability against agglomeration and detachment during electrochemical accelerated-aging protocols, which simulate the catalyst degradation occurring in PEM fuel cells. The increased ease of preparation and the flexibility of the new synthetic method could facilitate the use of such carbon supports in different areas of catalysis.

EXPERIMENTAL METHODS

Stöber Silica Spheres. A conventional Stöber process was used to prepare 200−220 nm silica spheres. A 60 mL portion of ethanol was mixed with 11.36 mL of ultrapure (mQ) water and 1.3 mL of aqueous ammonia solution (NH_3(aq), 28.0−30.0%). After the mixture stirred for 10 min, 2.38 mL of tetraethylorthosilicate (TEOS) was rapidly injected, and the reaction mixture was stirred for about 7 h. The initial ethanol/water (E/W) ratio is 5 (v/v) whereas the NH_3 and initial TEOS concentrations are 0.25 and 0.15 M, respectively.

Shell Deposition and HMCS. The reaction mixture composition (72.5 mL of total volume), which now contains 200 nm silica spheres, was adjusted by adding 183.1 mL of water and 37.2 mL of ethanol. After the mixture stirred for 15 min, 6 g of an aqueous cetyltrimethylammonium chloride solution (CTAC, 25 wt %) was added dropwise under vigorous stirring, to avoid agglomeration of the colloidal suspension. At this point, neglecting all the possible byproducts (EtOH and H_2O) formed during the hydrolysis and polycondensation of TEOS, the E/W ratio is 0.5 (v/v) whereas the NH_3 and CTAC concentrations are 59 mM and 15 mM, respectively. After the mixture stirred for 30 min, 0.62 g of resorcinol (19 mM) was added to the reaction mixture and stirred for dissolution for additional 30 min. At this point 0.84 mL of aqueous formaldehyde solution (37%) and 2.51 mL of TEOS were simultaneously added, and the reaction mixture was stirred overnight. For simplicity reasons, the reactant names are be abbreviated by their initials (resorcinol = R, formaldehyde = F, and TEOS = T). For all the experiments the R/F molar ratio was kept equal to 0.5. Four different T/R molar ratios were studied: 1 ([T] = 28.3 mM, [R] = 28.3 mM), 1.5 ([T] = 34.0 mM, [R] = 22.6 mM), 2 ([T] = 37.8 mM, [R] = 18.8 mM), and 3.5 ([T] = 44.1 mM; [R] = 12.6). The total amount of reactants (R + T) was kept constant and equal to 56.6 mM. After the mixture stirred for at least 12 h, the resulting colloidal suspension was directly transferred to Teflon-lined autoclaves, and it underwent a hydrothermal treatment (HT) for 24 h. Three different HT temperatures were chosen: 100, 120, and 150 °C, in addition to a sample separated before the HT. For the study of the influence of HT temperature, the initial T/R ratio during the shell deposition was set to 2 (mol/mol). After the treatment, the solid material was separated by centrifugation, rinsed with a mixture of ethanol/water (∼1:2), and dried at 50 °C. The carbonization was carried out in a tubular quartz furnace at 1000 °C (5 °C/min, 4 h of dwell time) under a N_2 atmosphere. The calcination (both starting from the polymer/silica and carbon/silica composites) was carried out in air under static conditions in a muffle furnace at 600 °C (2 °C/min, 1 h of dwell time). The silica framework was leached by leaving the carbon/silica composite in a 10% HF aqueous solution for at least 2 days. Once the solid powder has settled down, the supernatant solution was carefully removed, and the wet powder was washed again with water. This procedure was repeated twice, to make sure that the HF excess was completely removed. The carbon material (HMCS) was finally filtered, abundantly rinsed with deionized water, and dried at 75 °C. A reaction mixture volume of 300 mL (after the adjustment of the composition, E/W = 0.5) yields ∼3.2 g of silica@polymer/silica spheres, which in turn result in ∼1.2 g of silica@carbon/silica spheres and ∼0.25 g of HMCS.

Pt@HMCS. The procedure to encapsulate Pt nanoparticles (NPs) inside the porous framework of the hollow mesoporous carbon spheres (HMCS) followed the method previously developed in our group for metallic and bimetallic nanoparticles.[13] A detailed description is also reported in the Supporting Information.

Material Characterization. Gas physisorption measurements were carried out on a Micrometrics ASAP 2010 instrument. Prior to analysis, the materials were activated under vacuum for at least 8 h at 200 °C. For N_2 adsorption, the measurements were performed at 77.4 K using a static volumetric method, a 5% target tolerance, and 15 s for the equilibration intervals. For HMCS, an incremental-dose mode (30 cm^3/g, equilibration delay = 0.25−0.5 h) was employed in the low-pressure region (micropores). The BET surface area was calculated from the adsorption data in the relative pressure interval from 0.04 to 0.2. Unless otherwise specified, the pore size distribution (PSD) was estimated by the BJH (Barrett−Joyner−Halenda) method from the adsorption branch. The total pore volume (TPV) was estimated from the total N_2 uptake at the relative pressure of 0.98 p/p_0. The details about TEM and thermogravimetric analysis (TG) are reported in the Supporting Information.

Electrochemical Characterization. Electrochemical measurements were performed at room temperature in a three-compartment cell, using a rotating disk electrode (RDE) setup. Details about the setup configuration, catalyst film preparation, and experiment parameters (activity measurements) can be found in the Supporting Information. The accelerated degradation tests (ADT) up to 1.4 V consisted of 10 800 degradation cycles between 0.4 and 1.4 V_{RHE}, whereas the ADT up to 1.0 V included 360 activation cycles between 0.4 and 1.4 V_{RHE} followed by 10 440 degradation cycles between 0.4 and 1.0 V_{RHE}. The degradation tests were performed without rotation. In order to monitor the electrochemical surface area (ECSA) evolution during the degradation, CO-stripping was used to measure the real active area after 0, 360, 1080, 2160, 3600, 5400, 7200, and 10 800 potential cycles. The relative ECSA values are calculated normalizing the measured ECSA over the maximum value, typically obtained after 360 activation cycles.

ASSOCIATED CONTENT

Supporting Information

Additional details about Pt@HMCS synthesis and other characterization methods, further discussion of the silica counterpart textural properties (N_2 physisorption) and additional information about the influence of the T/R ratio, thermogravimetric analysis of polymer/silica composite spheres, details about N_2 and Ar physisorption analysis of HMCS, and comparison (TEM, XRD, electrochemical performance) of Pt@HMCS and Pt@HGS. The Supporting Information is available free of charge on the ACS Publications website at DOI: 10.1021/acsami.5b02580.

AUTHOR INFORMATION

Corresponding Author

*E-mail: schueth@kofo.mpg.de.

Notes

The authors declare no competing financial interest.

ACKNOWLEDGMENTS

The authors would like to thank the DFG for the financial support through DFG/AiF-Cluster "Innovative Materialen und Verfahren für MT-PEM-Brennstoffzellen". The "MaxNet Energy" consortium is acknowledged for supporting the collaborative work between MPI für Kohlenforschung and MPI für Eisenforschung. B. Spliethoff and H-J. Bongard, from the Electron Microscopy department at Max-Planck-Institut für Kohlenforschung headed by Prof. C. Lehmann, are gratefully acknowledged for the support in the TEM, STEM, and SEM measurements. Moreover, the authors would like to also thank Dipl.-Ing. A. Mingers for the help in the ICP-MS measure-

DOI: 10.1021/acsami.5b02580
ACS Appl. Mater. Interfaces 2015, 7, 12914−12922

ments. C.B. acknowledges financial support from the IMPRS-SurMat doctoral program.

REFERENCES

(1) Li, Y.; Shi, J. Hollow-Structured Mesoporous Materials: Chemical Synthesis, Functionalization and Applications. *Adv. Mater.* **2014**, *26*, 3176−3205.
(2) Argyo, C.; Weiss, V.; Bräuchle, C.; Bein, T. Multifunctional Mesoporous Silica Nanoparticles as a Universal Platform for Drug Delivery. *Chem. Mater.* **2014**, *26*, 435−451.
(3) Kim, M.; Sohn, K.; Na, H. B.; Hyeon, T. Synthesis of Nanorattles Composed of Gold Nanoparticles Encapsulated in Mesoporous Carbon and Polymer Shells. *Nano Lett.* **2002**, *2*, 1383−1387.
(4) Kim, J. Y.; Yoon, S. B.; Yu, J.-S. Fabrication of Nanocapsules with Au Particles Trapped inside Carbon and Silica Nanoporous shells. *Chem. Commun.* **2003**, 790−791.
(5) Fuertes, A. B.; Sevilla, M.; Valdes-Solis, T.; Tartaj, P. Synthetic Route to Nanocomposites Made up of Inorganic Nanoparticles Confined within a Hollow Mesoporous Carbon Shell. *Chem. Mater.* **2007**, *19*, 5418−5423.
(6) Guo, L.; Zhang, L.; Zhang, J.; Zhou, J.; He, Q.; Zeng, S.; Cui, X.; Shi, J. Hollow Mesoporous Carbon Spheres—an Excellent Bilirubin Adsorbent. *Chem. Commun.* **2009**, 6071−6073.
(7) Lee, I.; Joo, J. B.; Yin, Y.; Zaera, F. A Yolk@Shell Nanoarchitecture for Au/TiO2 Catalysts. *Angew. Chem., Int. Ed.* **2011**, *50*, 10208−10211.
(8) Liang, X.; Li, J.; Joo, J. B.; Gutiérrez, A.; Tillekaratne, A.; Lee, I.; Yin, Y.; Zaera, F. Diffusion through the Shells of Yolk-Shell and Core-Shell Nanostructures in the Liquid Phase. *Angew. Chem., Int. Ed.* **2012**, *51*, 8034−8036.
(9) Galeano, C.; Güttel, R.; Paul, M.; Arnal, P.; Lu, A.-H.; Schüth, F. Yolk-Shell Gold Nanoparticles as Model Materials for Support-Effect Studies in Heterogeneous Catalysis: Au,@ C and Au,@ ZrO2 for CO Oxidation as an Example. *Chem.—Eur. J.* **2011**, *17*, 8434−8439.
(10) Galeano, C.; Baldizzone, C.; Bongard, H.; Spliethoff, B.; Weidenthaler, C.; Meier, J. C.; Mayrhofer, K. J. J.; Schüth, F. Carbon-Based Yolk-Shell Materials for Fuel Cell Applications. *Adv. Funct. Mater.* **2014**, *24*, 220−232.
(11) Schüth, F. Encapsulation Strategies in Energy Conversion Materials. *Chem. Mater.* **2014**, *26*, 423−434.
(12) Chai, G. S.; Yoon, S. B.; Kim, J. H.; Yu, J.-S. Spherical Carbon Capsules with Hollow Macroporous Core and Mesoporous Shell Structures as a Highly Efficient Catalyst Support in the Direct Methanol Fuel Cell. *Chem. Commun.* **2004**, 2766−2767.
(13) Galeano, C.; Meier, J. C.; Peinecke, V.; Bongard, H.; Katsounaros, I.; Topalov, A. A.; Lu, A.; Mayrhofer, K. J. J.; Schüth, F. Toward Highly Stable Electrocatalysts via Nanoparticle Pore Confinement. *J. Am. Chem. Soc.* **2012**, *134*, 20457−20465.
(14) Lu, A.-H.; Hao, G.-P.; Sun, Q.; Zhang, X.-Q.; Li, W.-C. Chemical Synthesis of Carbon Materials With Intriguing Nanostructure and Morphology. *Macromol. Chem. Phys.* **2012**, *213*, 1107−1131.
(15) Yoon, S. B.; Sohn, K.; Kim, J. Y.; Shin, C.-H.; Yu, J.-S.; Hyeon, T. Fabrication of Carbon Capsules with Hollow Macroporous Core/Mesoporous Shell Structures. *Adv. Mater.* **2002**, *14*, 19−21.
(16) Valle-Vigón, P.; Sevilla, M.; Fuertes, A. B. Synthesis of Uniform Mesoporous Carbon Capsules by Carbonization of Organosilica Nanospheres. *Chem. Mater.* **2010**, *22*, 2526−2533.
(17) Zhao, W.; Shi, J.; Chen, H.; Zhang, L. Particle Size, Uniformity, and Mesostructure Control of Magnetic Core/mesoporous Silica Shell Nanocomposite Spheres. *J. Mater. Res.* **2006**, *21*, 3080−3089.
(18) Tatsuda, N.; Yano, K. Pore Size Control of Monodispersed Starburst Carbon Spheres. *Carbon* **2013**, *51*, 27−35.
(19) Mizutani, M.; Yamada, Y.; Yano, K. Pore-Expansion of Monodisperse Mesoporous Silica Spheres by a Novel Surfactant Exchange Method. *Chem. Commun.* **2007**, 1172−1174.
(20) Baldizzone, C.; Mezzavilla, S.; Carvalho, H. W. P.; Meier, J. C.; Schuppert, A. K.; Heggen, M.; Galeano, C.; Grunwaldt, J.-D.; Schüth, F.; Mayrhofer, K. J. J. Confined-Space Alloying of Nanoparticles for the Synthesis of Efficient PtNi Fuel-Cell Catalysts. *Angew. Chem., Int. Ed.* **2014**, *53*, 14250−14254.
(21) Haraguchi, K.; Usami, Y.; Yamamura, K.; Matsumoto, S. Morphological Investigation of Hybrid Materials Composed of Phenolic Resin and Silica Prepared by in Situ Polymerization. *Polymer* **1998**, *39*, 6243−6250.
(22) Lin, J. M.; Ma, C. C. M.; Wang, F. Y.; Wu, H. D.; Kuang, S. C. Thermal, Mechanical, and Morphological Properties of Phenolic Resin/silica Hybrid Ceramers. *J. Polym. Sci., Part B: Polym. Phys.* **2000**, *38*, 1699−1706.
(23) Lee, J.; Kim, J.; Lee, Y.; Yoon, S.; Oh, S. M.; Hyeon, T. Simple Synthesis of Uniform Mesoporous Carbons with Diverse Structures from Mesostructured Polymer/Silica Nanocomposites. *Chem. Mater.* **2004**, *16*, 3323−3330.
(24) Hernández-Padrón, G.; Rojas, F.; Castaño, V. M. Ordered SiO_2−(phenolic-Formaldehyde Resin) *in Situ* Nanocomposites. *Nanotechnology* **2004**, *15*, 98−103.
(25) Ye, L.; Ji, Z.-H.; Han, W.-J.; Hu, J.-D.; Zhao, T. Synthesis and Characterization of Silica/Carbon Composite Aerogels. *J. Am. Ceram. Soc.* **2010**, *93*, 1156−1163.
(26) Li, Y.; Wei, J.; Luo, W.; Wang, C.; Li, W.; Feng, S.; Yue, Q.; Wang, M.; Elzatahry, A. A.; Deng, Y.; Zhao, D. Tricomponent Coassembly Approach To Synthesize Ordered Mesoporous Carbon/Silica Nanocomposites and Their Derivative Mesoporous Silicas with Dual Porosities. *Chem. Mater.* **2014**, *26*, 2438−2444.
(27) Si, M.; Feng, D.; Qiu, L.; Jia, D.; Elzatahry, A. A.; Zheng, G.; Zhao, D. Free-Standing Highly Ordered Mesoporous Carbon−silica Composite Thin Films. *J. Mater. Chem. A* **2013**, *1*, 13490−13495.
(28) Liu, J.; Qiao, S. Z.; Liu, H.; Chen, J.; Orpe, A.; Zhao, D.; Lu, G. Q. M. Extension of The Stöber Method to the Preparation of Monodisperse Resorcinol-Formaldehyde Resin Polymer and Carbon Spheres. *Angew. Chem., Int. Ed.* **2011**, *50*, 5947−5951.
(29) Zhang, X.; Li, Y.; Cao, C. Facile One-Pot Synthesis of Mesoporous Hierarchically Structured Silica/carbon Nanomaterials. *J. Mater. Chem.* **2012**, *22*, 13918−13921.
(30) Qiao, Z.-A.; Guo, B.; Binder, A. J.; Chen, J.; Veith, G. M.; Dai, S. Controlled Synthesis of Mesoporous Carbon Nanostructures via a "Silica-Assisted" Strategy. *Nano Lett.* **2013**, *13*, 207−212.
(31) Wang, J.; Feng, S.; Song, Y.; Li, W.; Gao, W.; Elzatahry, A. A.; Aldhayan, D.; Xia, Y.; Zhao, D. Synthesis of Hierarchically Porous Carbon Spheres with Yolk-Shell Structure for High Performance Supercapacitors. *Catal. Today* **2015**, *243*, 199−208.
(32) Giesche, H. Synthesis of Monodispersed Silica Powders I. Particle Properties and Reaction Kinetics. *J. Eur. Ceram. Soc.* **1994**, *14*, 189−204.
(33) Liu, R.; Shi, Y.; Wan, Y.; Meng, Y.; Zhang, F.; Gu, D.; Chen, Z.; Tu, B.; Zhao, D. Triconstituent Co-Assembly to Ordered Mesostructured Polymer−Silica and Carbon−Silica Nanocomposites and Large-Pore Mesoporous Carbons with High Surface Areas. *J. Am. Chem. Soc.* **2006**, *128*, 11652−11662.
(34) Leboda, R.; Mendyk, E. Hydrothermal Modification of Porous Structure of Silica Adsorbents. *Mater. Chem. Phys.* **1991**, *27*, 189−212.
(35) Kleitz, F. Ordered Mesoporous Materials. In *Handbook of Heterogeneous Catalysis*; Ertl, G., Knözinger, H., Schüth, F., Weitkamp, J., Eds.; Wiley-VCH: New York, 2008.
(36) Huang, Y.; Cai, H.; Feng, D.; Gu, D.; Deng, Y.; Tu, B.; Wang, H.; Webley, P. A.; Zhao, D. One-Step Hydrothermal Synthesis of Ordered Mesostructured Carbonaceous Monoliths with Hierarchical Porosities. *Chem. Commun.* **2008**, 2641−2643.
(37) Muylaert, I.; Verberckmoes, A.; De Decker, J.; Van Der Voort, P. Ordered Mesoporous Phenolic Resins: Highly Versatile and Ultra Stable Support Materials. *Adv. Colloid Interface Sci.* **2012**, *175*, 39−51.
(38) Fuertes, A. B.; Valle-Vigón, P.; Sevilla, M. One-Step Synthesis of Silica@resorcinol−formaldehyde Spheres and Their Application for the Fabrication of Polymer and Carbon Capsules. *Chem. Commun.* **2012**, *48*, 6124−6126.
(39) Liu, R.; Qu, F.; Guo, Y.; Yao, N.; Priestley, R. D. Au@carbon Yolk−shell Nanostructures via One-Step Core−shell−shell Template. *Chem. Commun.* **2014**, *50*, 478−480.

DOI: 10.1021/acsami.5b02580
ACS Appl. Mater. Interfaces 2015, 7, 12914−12922

(40) Liu, R.; Yeh, Y.-W.; Tam, V. H.; Qu, F.; Yao, N.; Priestley, R. D. One-Pot Stöber Route Yields Template for Ag@carbon Yolk−shell Nanostructures. *Chem. Commun.* **2014**, *50*, 9056−9059.
(41) Wu, Z.; Wu, W. D.; Liu, W.; Selomulya, C.; Chen, X. D.; Zhao, D. A General "Surface-Locking" Approach toward Fast Assembly and Processing of Large-Sized, Ordered, Mesoporous Carbon Microspheres. *Angew. Chem., Int. Ed.* **2013**, *52*, 13764−13768.
(42) Thommes, M. Physical Adsorption Characterization of Nanoporous Materials. *Chem. Ing. Tech.* **2010**, *82*, 1059−1073.
(43) Chen, Y.; Chen, H.; Guo, L.; He, Q.; Chen, F.; Zhou, J.; Feng, J.; Shi, J. Hollow/Rattle-Type Mesoporous Nanostructures by a Structural Difference-Based Selective Etching Strategy. *ACS Nano* **2010**, *4*, 529−539.
(44) Yu, Q.; Hui, J.; Wang, P.; Xu, B.; Zhuang, J.; Wang, X. Hydrothermal Synthesis of Mesoporous Silica Spheres: Effect of the Cooling Process. *Nanoscale* **2012**, *4*, 7114−7120.
(45) Durairaj, R. B. *Resorcinol: Chemistry, Technology, and Applications*; Springer: Berlin, 2005.
(46) Onori, G.; Santucci, A. Effect of 1-Alcohols on Micelle Formation and Hydrophobic Interactions. *Trends in Colloid and Interface Science VI*; Wiley: New York, 1992; pp 297−301.
(47) Li, W.; Zhang, M.; Zhang, J.; Han, Y. Self-Assembly of Cetyl Trimethylammonium Bromide in Ethanol-Water Mixtures. *Front. Chem. China* **2006**, *1*, 438−442.
(48) Brinker, C. J.; Scherer, G. W. *Sol-gel science: the physics and chemistry of sol-gel processing*; Academic Press: 1990.
(49) Meier, J. C.; Galeano, C.; Katsounaros, I.; Witte, J.; Bongard, H. J.; Topalov, A. A.; Baldizzone, C.; Mezzavilla, S.; Schüth, F.; Mayrhofer, K. J. J. Design Criteria for Stable Pt/C Fuel Cell Catalysts. *Beilstein J. Nanotechnol.* **2014**, *5*, 44−67.
(50) Nesselberger, M.; Ashton, S.; Meier, J. C.; Katsounaros, I.; Mayrhofer, K. J. J.; Arenz, M. The Particle Size Effect on the Oxygen Reduction Reaction Activity of Pt Catalysts: Influence of Electrolyte and Relation to Single Crystal Models. *J. Am. Chem. Soc.* **2011**, *133*, 17428−17433.
(51) Makharia, R.; Kocha, S.; Yu, P.; Sweikart, M. A.; Gu, W.; Wagner, F.; Gasteiger, H. A. Durable PEM Fuel Cell Electrode Materials: Requirements and Benchmarking Methodologies. *ECS Trans.* **2006**, *1*, 3−18.
(52) Shao-Horn, Y.; Sheng, W. C.; Chen, S.; Ferreira, P. J.; Holby, E. F.; Morgan, D. Instability of Supported Platinum Nanoparticles in Low-Temperature Fuel Cells. *Top. Catal.* **2007**, *46*, 285−305.

DOI: 10.1021/acsami.5b02580
ACS Appl. Mater. Interfaces 2015, 7, 12914−12922